Supplementary Information for

High-performance transparent metal mesh electrodes utilizing a metal-vapor-desorption layer for organic light-emitting diode applications

Dahyun Kim[1,2], Sujin Jeong[1,2], Dong Keon Lee[1,2], Wonjune Yi[1,2], Hyungsoo Yoon[1,2], Joohee Jeon[1,2], Hayun Kim[1,2], Byeongmoon Lee[3], and Yongtaek Hong[1,2*]*

[1]Department of Electrical and Computer Engineering, Seoul National University, Seoul 08826, Korea

[2]Inter-university Semiconductor Research Center (ISRC), Seoul National University, Seoul 08826, Korea

[3]Department of Electrical Engineering and Computer Science, Daegu Gyeongbuk Institute of Science and Technology (DGIST), Daegu 42988, Korea

KEYWORDS: transparent electrodes, selective deposition, transfer printing, organic light-emitting diodes (OLEDs), metal-vapor-desorption layer

Supplementary Information

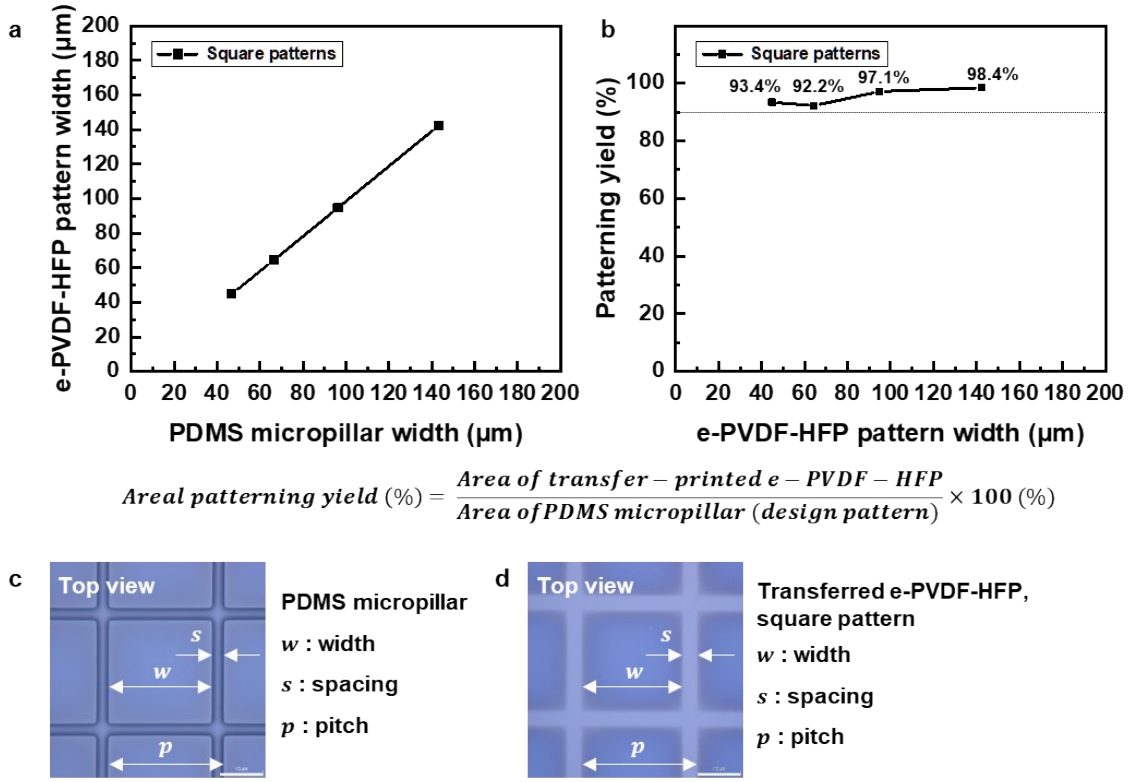

$$Areal\ patterning\ yield\ (\%) = \frac{Area\ of\ transfer-printed\ e-PVDF-HFP}{Area\ of\ PDMS\ micropillar\ (design\ pattern)} \times 100\ (\%)$$

Figure S1. Transfer printing of e-PVDF-HFP pattern (a) square pattern width of PDMS micropillar stamp and corresponding square pattern width of transferred e-PVDF-HFP (b) areal patterning yield of square patterns with different e-PVDF-HFP pattern widths. (c) Optical images representing the width, spacing, and pitch of the PDMS micropillar stamp and (d) transferred e-PVDF-HFP pattern

Table S1. Detailed data of the width, spacing, and pitch of the PDMS micropillar stamp and the corresponding width, spacing, and pitch of transferred e-PVDF-HFP pattern, and the calculated areal patterning yield of each square pattern

No.	PDMS micropillar			Transferred e-PVDF-HFP film, square pattern [μm]			Areal patterning yield (%)
	Width [μm]	Spacing [μm]	Pitch [μm]	Width [μm]	Spacing [μm]	Pitch [μm]	
1	46.8	11.7	58.5	44.8	14.8	59.6	93.3711%
2	66.4	11.7	78.1	64.4	14.4	78.9	92.2094%
3	96.2	11.8	108.0	94.7	12.9	107.7	97.1144%
4	143.2	12.0	155.2	142.3	14.6	156.9	98.4169%

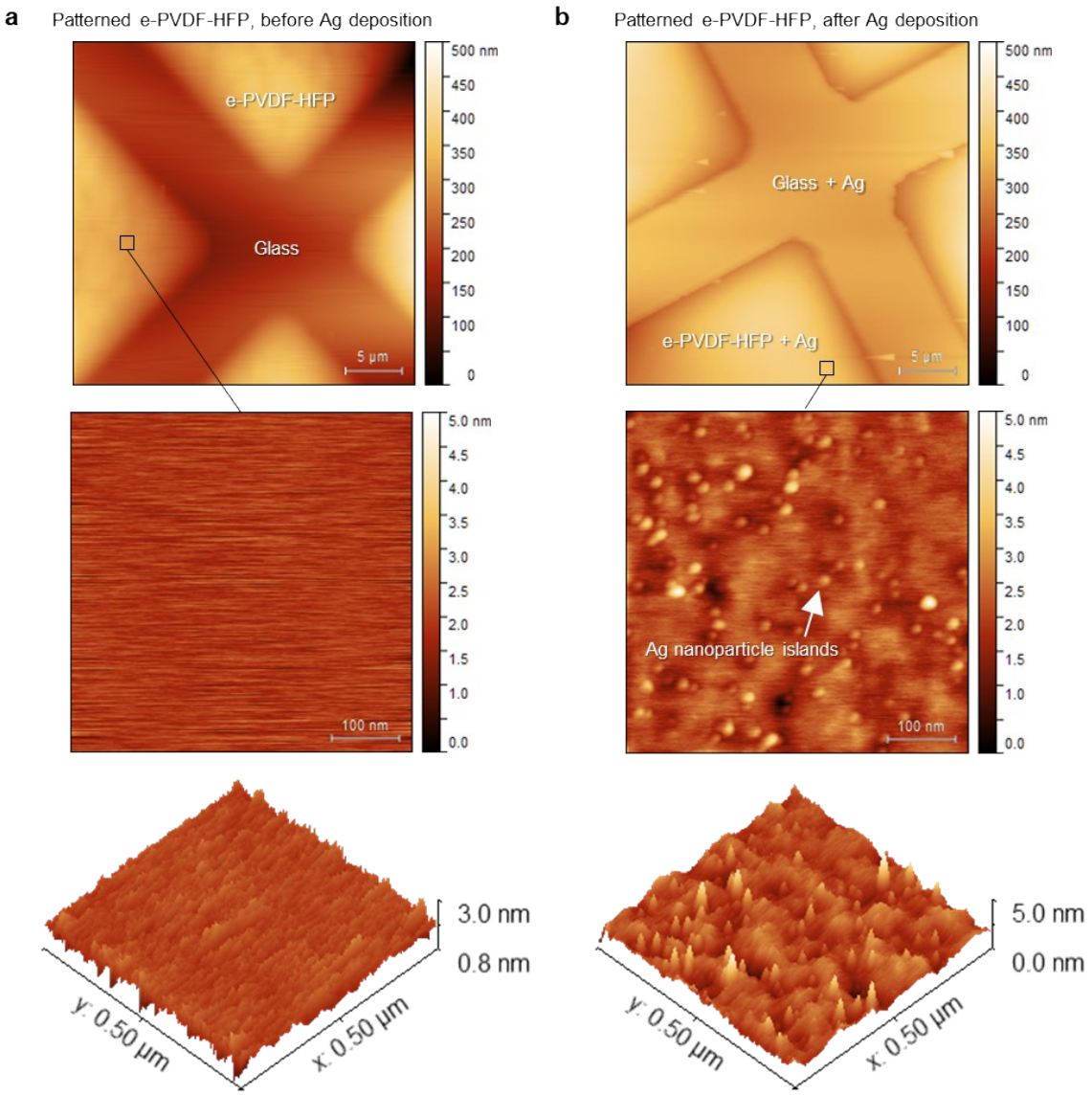

Figure S2. AFM images of fabricated metal mesh electrodes on glass substrate (a) before and (b) after Ag (100 nm) deposition.

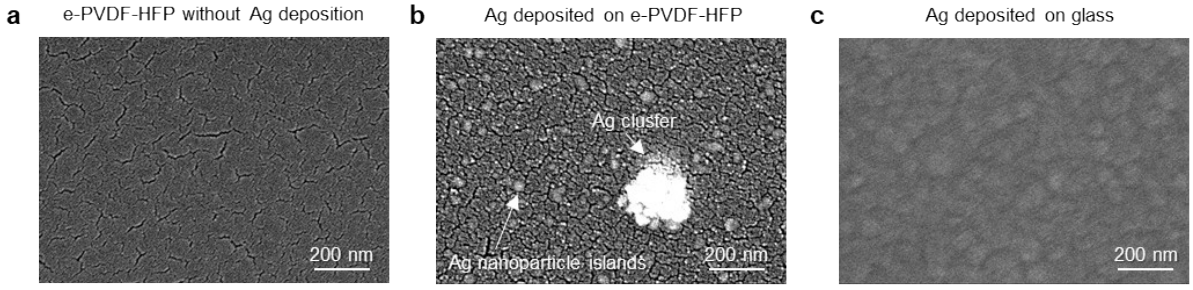

Figure S3. FE-SEM images of (a) e-PVDF-HFP without Ag deposition, (b) Ag (300 nm) deposited on e-PVDF-HFP and (c) on glass substrate.

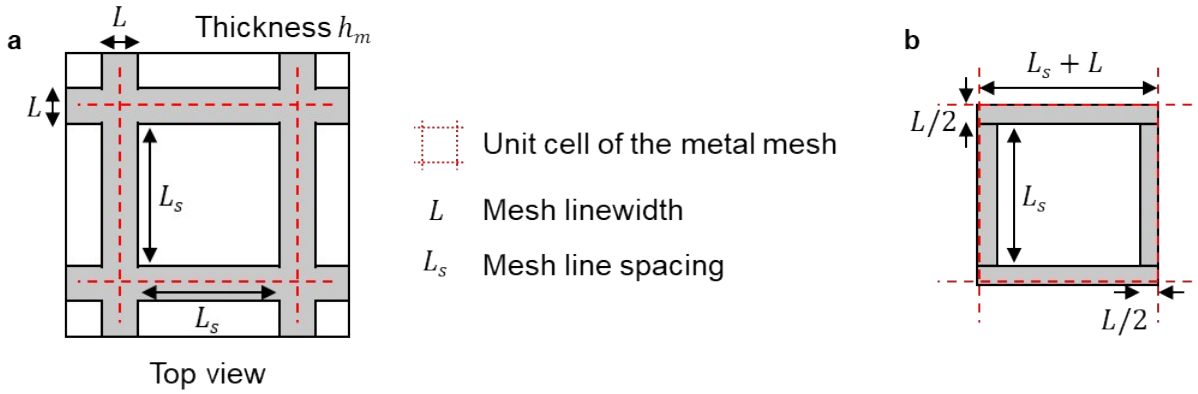

Figure S4. Schematic image representing (a) the geometrical parameters of the metal mesh electrode and (b) the parameters used for calculation based on a unit cell of the metal mesh electrode

Supplementary Note 1. Theoretical analysis of the FoM

Theoretical analysis of the FoM based on the idealized calculation of the transmittance and the sheet resistance of mesh-patterned metal films were derived as follows. Here, The sheet resistance was calculated following the analytical framework reported in the previous report[1], also 100% transmittance in the e-PVDF-HFP region and 0% transmittance in the metal mesh region were assumed. The metal mesh is assumed to be perfectly periodic, as illustrated in Figure S4.

Based on Ohm's law and from its geometry, the ideal sheet resistance (R_s) and transmittance (T) of the metal mesh can be theoretically written as follows,

$$R_s = \xi \frac{\rho}{h_m}\left(\frac{L}{L_s + L} + \frac{L_s}{L}\right)$$

$$T = \left(\frac{L_s}{L_s + L}\right)^2 = \left(\frac{1}{1 + (L/L_s)}\right)^2$$

where ρ and h_m are the resistivity and thickness of the metal film, respectively. ξ is a correlation factor, which can be determined experimentally. L and L_s are the mesh linewidth and line spacing, respectively. (Figure S4)

Overall, FoM[2-5] for the transparent conducting electrodes can be calculated using the results above as follows. It is noted that as L decreases or L_s widens, the FoM is expected to increase.

$$FoM = \frac{188.5}{R_s\left(T^{-1/2} - 1\right)} = \frac{188.5\, h_m}{\xi\rho}\left(\frac{(\frac{L}{L_s})^2}{(1 + \frac{L}{L_s})} + 1\right)^{-1}$$

References

[1] D. S. Ghosh, T. L. Chen and V. Pruneri, *Appl. Phys. Lett.*, 2010, **96**, 041109.

[2] M. Dressel and G. Gruner, Electrodynamics of Solids: Optical Properties of Electrons in Matter, *Cambridge University Press*, Cambridge, 2002.

[3] L. Hu, D. S. Hecht and G. Grüner, *Nano Letters*, 2004, **4**, 2513-2517.

[4] S. De and J. N. Coleman, *ACS Nano*, 2010, **4**, 2713.

[5] Á. Pekker and K. Kamarás, *Journal of Applied Physics*, 2010, **108**, 054318.

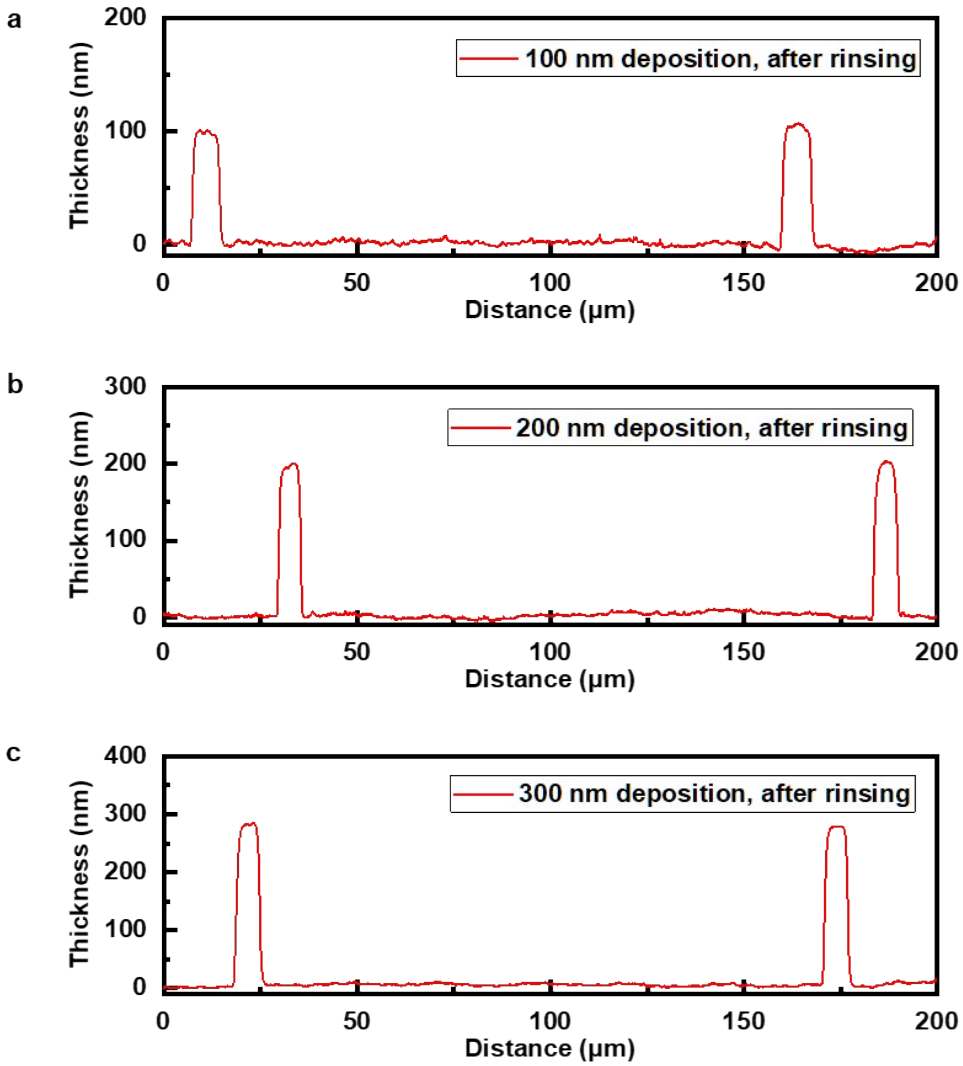

Figure S5. Surface profiles of fabricated metal mesh electrodes on glass substrate, measured after removing e-PVDF-HFP patterns by rinsing. Ag deposition thickness of (a) 100 nm, (b) 200 nm, and (c) 300 nm. The surface profiles were measured using a stylus profilometer (DektakXT-A, Bruker).

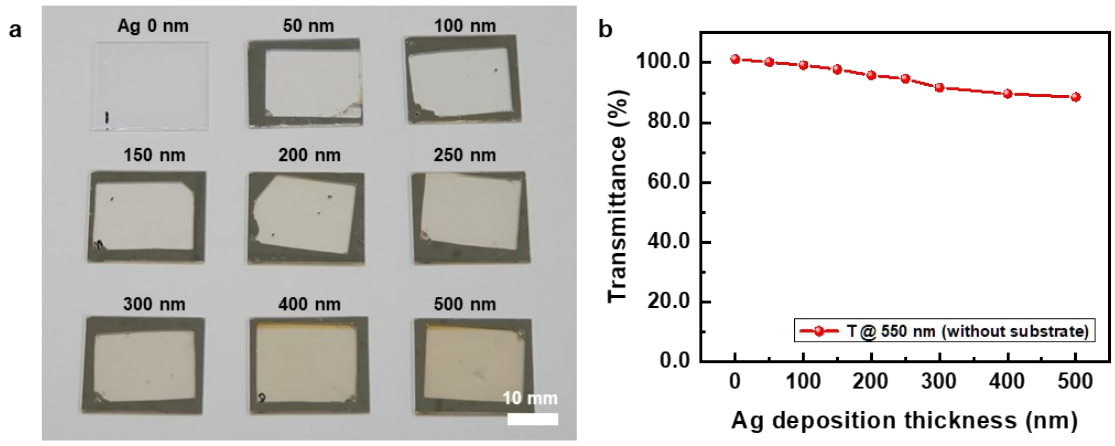

Figure S6. (a) Photographs of non-patterned e-PVDF-HFP films transferred to a glass substrate, with different Ag deposition thicknesses. (b) Measured transmittance (at 550 nm) of non-patterned e-PVDF-HFP films transferred to a glass substrate, with different Ag deposition thicknesses.

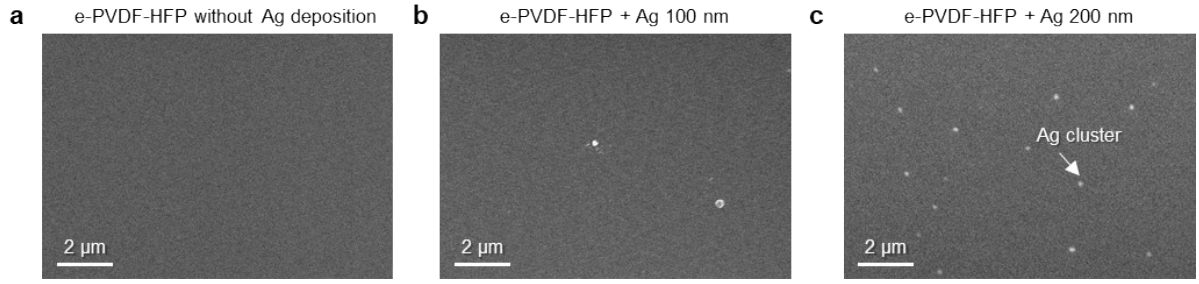

Figure S7. FE-SEM images of e-PVDF-HFP with different Ag deposition thicknesses, indicating increased growth of Ag clusters as Ag deposition thicknesses increased. (a) 0 nm (without Ag deposition), (b) 100 nm, and (c) 200 nm.

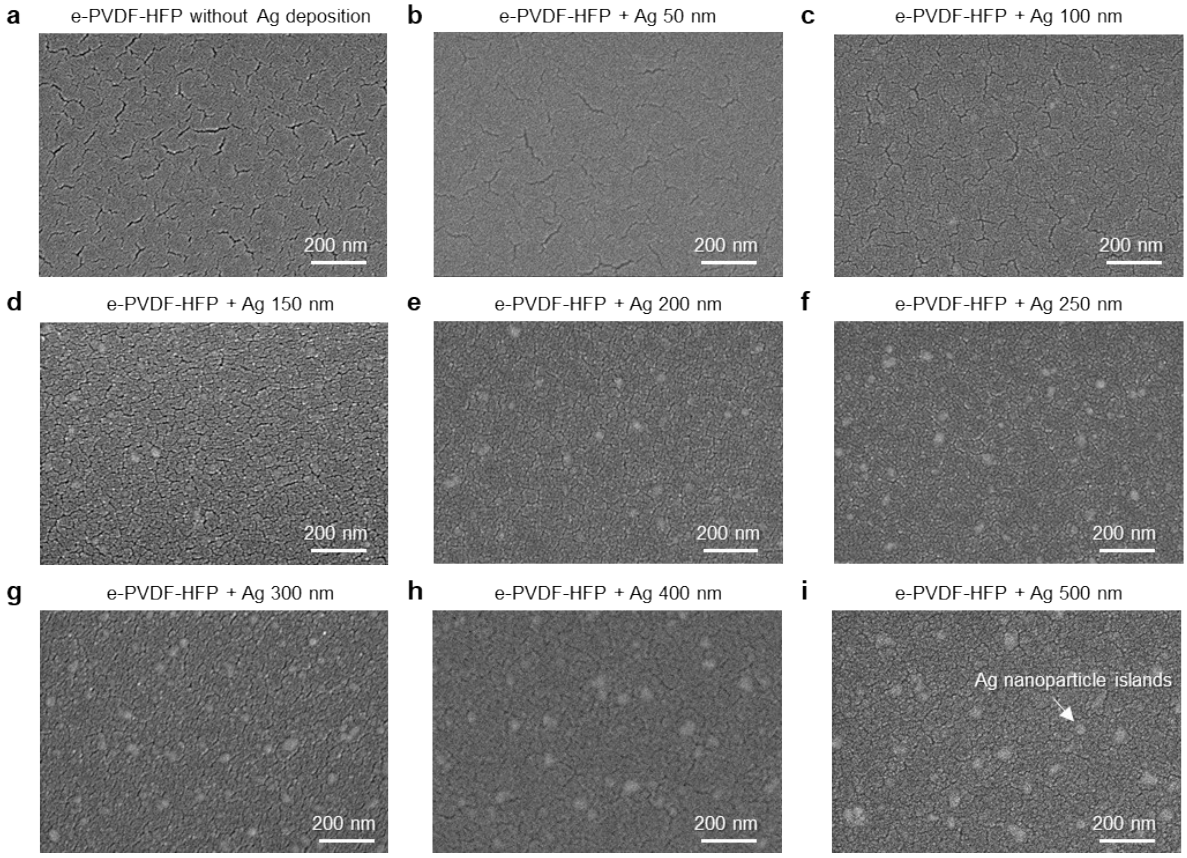

Figure S8. FE-SEM images of e-PVDF-HFP with different Ag deposition thicknesses, indicating increased growth of Ag nanoparticle islands as Ag deposition thicknesses increased. (a) 0 nm (without Ag deposition), (b) 50 nm, (c) 100 nm, (d) 150 nm, (e) 200 nm, (f) 250 nm, (g) 300 nm, (h) 400 nm, and (i) 500 nm.

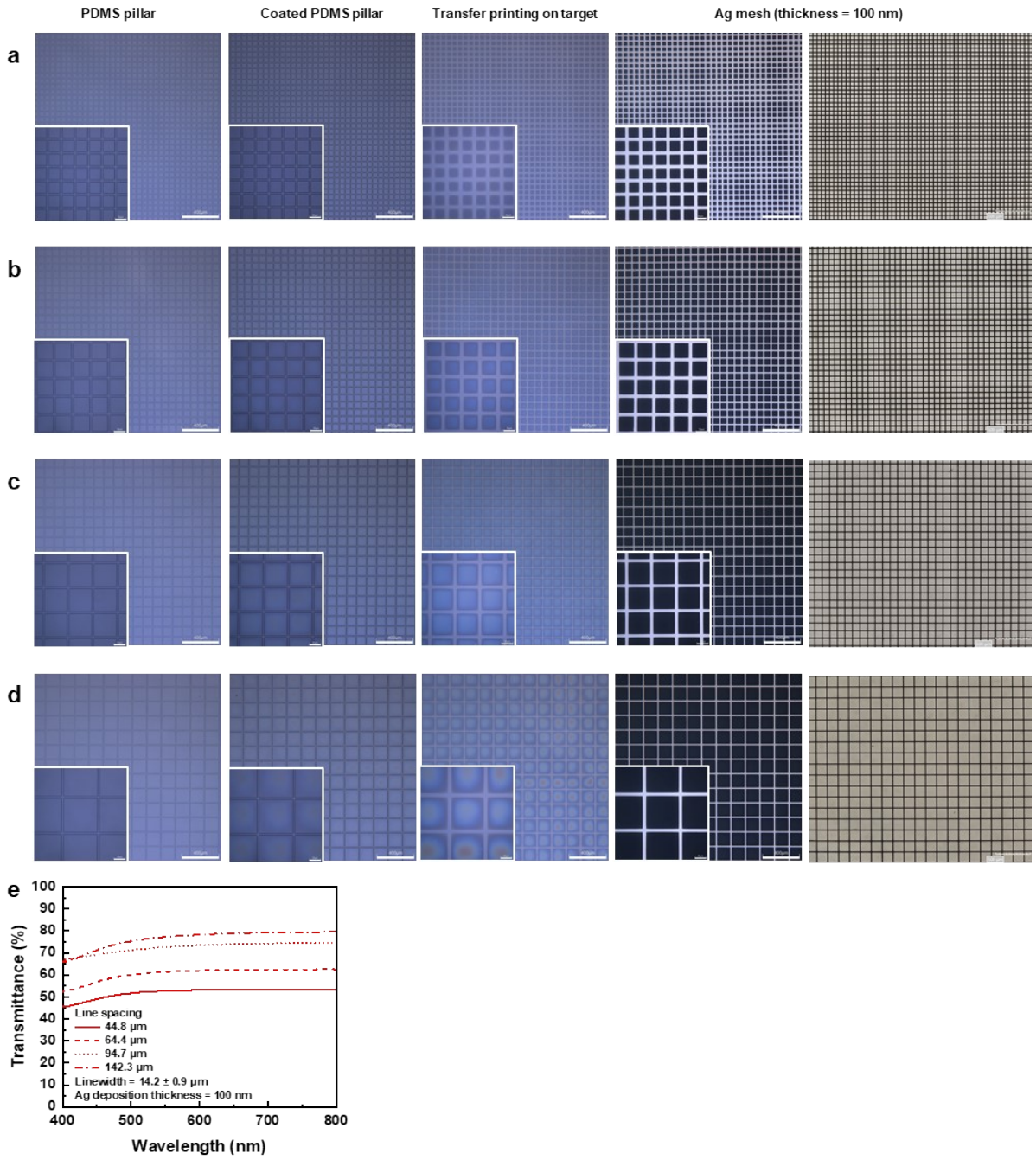

Figure S9. Metal mesh with different line spacing (a)-(d) Optical microscopic image (e) Transmittance

Table S2. Detailed data of metal mesh with different line spacing

	Line spacing (μm)	Mesh linewidth (μm)	Mesh pitch (μm)	e-PVDF-HFP pattern height (nm)	Ag thickness (nm)	%T	Rs (ohm/sq)	Haze (%)	FoM (σ_{dc}/σ_{op}) [1]	FoM (Haacke, x10^{-3}) [2]
a	44.8	14.8	59.6	80.6	100	57.5	0.887	5.6	666.0	4.4
b	64.4	14.4	78.9	99.7	100	66.9	1.148	3.9	737.3	15.6
c	94.7	12.9	107.7	103.35	100	79.1	1.566	2.7	970.3	61.6
d	142.3	14.6	156.9	129.8	100	84.2	1.872	1.8	1117.7	95.2

References

[1] M. Dressel and G. Grüner, Electrodynamics of Solids: Optical Properties of Electrons in Matter, Cambridge University Press, Cambridge, 2002.

[2] G. Haacke, J. Appl. Phys., 1976, 47, 4086-4089.

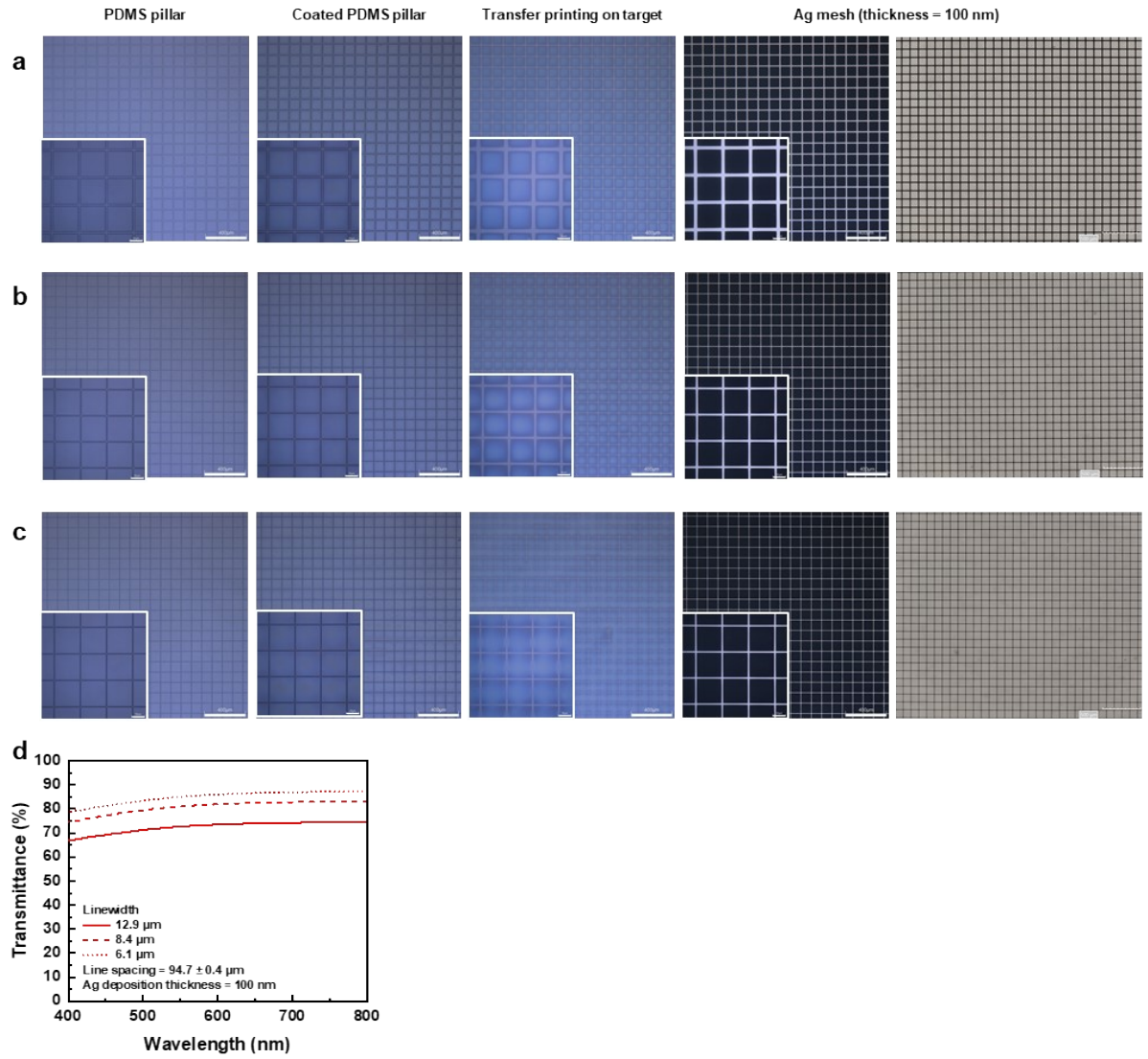

Figure S10. Metal mesh with different linewidth (a)-(c) Optical microscopic image (d) Transmittance

Table S3. Detailed data of metal mesh with different linewidth

	Line spacing (μm)	Mesh linewidth (μm)	Mesh pitch (μm)	e-PVDF-HFP pattern height (nm)	Ag thickness (nm)	%T	Rs (ohm/sq)	Haze (%)	FoM (σ_{dc}/σ_{op}) [1]	FoM (Haacke, x10^{-3}) [2]
a	94.7	12.9	107.7	92.8	100	79.1	1.566	2.7	970.3	61.6
b	94.4	8.4	102.8	127	100	88.3	2.632	2.8	1114.6	109.3
c	95.1	6.1	101.2	134.6	100	92.6	3.903	2.9	1229.9	118.6

References

[1] M. Dressel and G. Grüner, Electrodynamics of Solids: Optical Properties of Electrons in Matter, Cambridge University Press, Cambridge, 2002.

[2] G. Haacke, J. Appl. Phys., 1976, 47, 4086-4089.

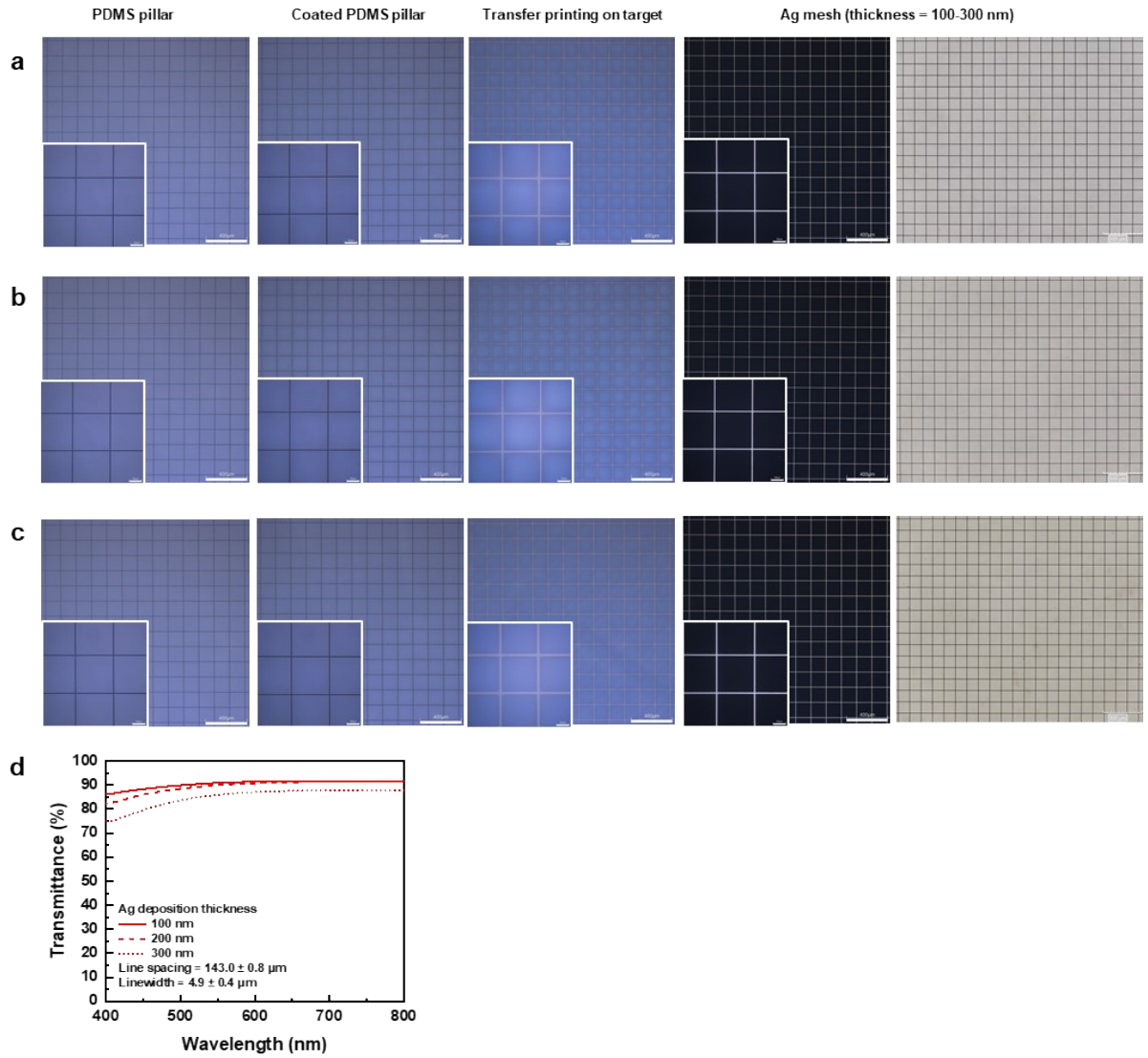

Figure S11. Metal mesh with different thickness (a)-(c) Optical microscopic image (d) Transmittance

Table S4. Detailed data of metal mesh with different thickness

	Line spacing (μm)	Mesh linewidth (μm)	Mesh pitch (μm)	Ag thickness (nm)	%T	Rs (ohm/sq)	Haze (%)	FoM (σ_{dc}/σ_{op}) [1]	FoM (Haacke, x10^{-3}) [2]
a	142.9	4.7	147.7	100	99.0	4.443	1.8	8866.4	204.6
b	143.9	4.7	148.6	200	98.0	1.777	1.9	10756.4	462.4
c	142.3	5.4	147.6	300	93.6	1.115	2.4	5038.1	463.5

References

[1] M. Dressel and G. Grüner, Electrodynamics of Solids: Optical Properties of Electrons in Matter, Cambridge University Press, Cambridge, 2002.

[2] G. Haacke, J. Appl. Phys., 1976, 47, 4086-4089.

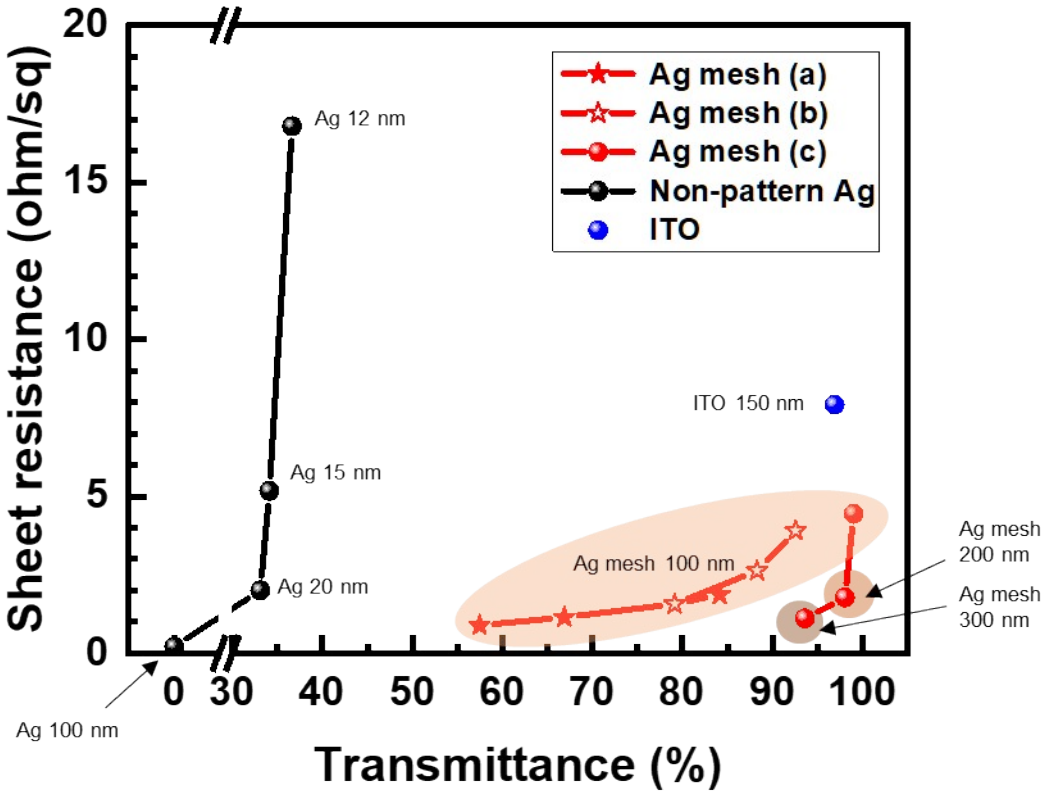

Figure S12. Comparison of measured transmittance and sheet resistance of fabricated metal mesh to non-patterned metal and commercial ITO glass

Table S5. Measured transmittance and sheet resistance of fabricated metal mesh with different line spacing, linewidth or thickness

Metal mesh group		Linewidth (μm)	Line spacing (μm)	Thickness (nm)	Transmittance (%)	Sheet Resistance (ohm/sq)
Line spacing	A1	14.8	44.8	100	57.5	0.887
	A2	14.4	64.4	100	66.9	1.15
	A3	14.6	142.3	100	84.2	1.87
Linewidth	B1	12.9	94.7	100	79.1	1.57
	B2	8.4	94.4	100	88.3	2.63
	B3	6.1	95.1	100	92.6	3.90
Thickness	C1	4.7	142.9	100	99.0	4.44
	C2	4.7	143.9	200	98.1	1.78
	C3	5.4	142.3	300	93.6	1.11

Table S6. Comparison of transmittance, sheet resistance, and figure of merits to previous studies with high-performance thin-film transparent electrodes incorporating transparent conductive oxides[1, 2], ultrathin metal films[3, 4], D/M/D multilayers[5, 6], AgNWs[7, 8], graphene[9], CNT[10], evaporated[11, 12] or printed[13, 14] metal mesh.

Ref#	Electrode	Year	Fabrication method	Transmittance (%T)	Sheet resistance (ohm/sq)	Figure of merit (σ_{dc}/σ_{op}) [15]	Figure of merit (T^{10}/Rs, x10^{-3}) [16]
[1]	Transparent Conducting Oxides	2000	Pulsed laser deposition (PLD) ITO	88.05-95.12	7-58	61.7-409.9	6.17-40.01
[2]		2021	Sputtering IZO	75.07-88.96	11.44-48.75	37.8-273.5	2.24-27.13
[3]	Ultrathin metal films	2020	TPBi/Ca/Ag 30/3/8-11nm Deposition	58.5-74.5	5.5-8.8	111.5-135.1	0.85-5.99
[4]		2025	ZnO/Yb:Ag(6%) 3/13-19nm Deposition	77.6-86.8	11.1-16.8	123.0-221.0	7.16-20.86
[5]	D/M/D multilayers	2020	ITO/Ag/ITO 35/8/12nm (simulation) or ZnO/Ag/ZnO 47/6/12nm (simulation)	95.4-95.5	4.7-7.14	1108.1-1722.1	87.46-134.26
[6]		2006	ZnO/Ag/ZnO 20/5-8/20nm Sputtering	88.0-95.5	0.8-3.5	1374.3-3569.9	132.45-348.13
[7]	Aligned AgNWs	2023	AgNW direct writing (using triple conical fibers)	95.8-98.5	12.5-25.5	604.6-974.5	33.71-52.09
[8]		2022	AgNW EHD printing	89.7-99.1	5.4-91	430.4-625.0	10.04-62.45
[9]	Graphene or CNT	2025	Graphene, CVD + transfer + PMMA removing in water	92.3-97.2	288-713.5	14.2-18.5	1.06-1.56
[10]		2019	DWCNT, slot-die coating + acid treatment	85.3-98.2	145-968.8	15.7-24.4	0.86-1.72
[11]	Evaporated metal mesh	2021	Cu deposition + HDT pattern uCP	80.3-92.1	3.1-9.6	446.9-524.4	34.82-45.74
[12]		2023	Ag, Selective deposition	77.5-91.5	2.2-7.6	371.1-630.4	32.81-54.12
[13]	Printed metal mesh	2023	AgNP Inkjet Printing	79.6-89.3	5.6-16.3	198.6-306.5	18.24-26.51
[14]		2018	AgNP Reverse-offset Printing	76.5-93.2	6.1-17	215.6-353.9	11.25-34.22
Our work	Evaporated metal mesh	2025	Transfer printing + Selective deposition, Ag	93.6-99.0	1.11-4.44	5038.1-10756.4	204.6-463.5

References

[1] H. Kim, J. S. Horwitz, G. Kushto, A. Piqué, Z. H. Kafafi, C. M. Gilmore and D. B. Chrisey, *J. Appl. Phys.*, 2000, **88**, 6021-6025.

[2] Z. Ying, Y. Zhu, X. Feng, J. Xiu, R. Zhang, X. Ma, Y. Deng, H. Pan and Z. He, *Adv. Mater. Interfaces*, 2021, **8**, 2001604.

[3] D. Yin, Z.-Y. Chen, N.-R. Jiang, Y.-F. Liu, Y.-G. Bi, X.-L. Zhang, W. Han, J. Feng and H.-B. Sun, *Org. Electron.*, 2020, **76**, 105494.

[4] E.-y. Choi, S.-C. Kang, K. Kim, S.-H. Lee, J.-B. Kim and J.-K. Song, *Light Sci. Appl.*, 2025, **14**, 62.

[5] H. Ferhati and F. Djeffal, *J. Comput. Electron.*, 2020, **19**, 815-824.

[6] D. R. Sahu, S.-Y. Lin and J.-L. Huang, *Appl. Surf. Sci.*, 2006, **252**, 7509-7514.

[7] K. Zhang, L. Meng, M. Zhang, Y. Li, L. Jiang and H. Liu, *Adv. Funct. Mater.*, 2024, **34**, 2308468.

[8] X. Feng, L. Wang, Y. Y. S. Huang, Y. Luo, J. Ba, H. H. Shi, Y. Pei, S. Zhang, Z. Zhang, X. Jia and B. Lu, *ACS Appl. Mater. Interfaces*, 2022, **14**, 39199-39210.

[9] B. Kulyk, J. C. Germino, D. Gaspar, A. J. S. Fernandes, J. Deuermeier, A. F. Carvalho, A. F. da Cunha, L. M. N. Pereira, L. Pereira and F. M. Costa, *J. Mater. Chem. C*, 2025, **13**, 5855-5864.

[10] I. Jeon, J. Yoon, U. Kim, C. Lee, R. Xiang, A. Shawky, J. Xi, J. Byeon, H. M. Lee, M. Choi, S. Maruyama and Y. Matsuo, *Adv. Energy Mater.*, 2019, **9**, 1901204.

[11] P. Bellchambers, S. Varagnolo, C. Maltby and R. A. Hatton, *ACS Appl. Energy Mater.*, 2021, **4**, 4150-4155.

[12] P. Bellchambers, C. Henderson, S. Abrahamczyk, S. Choi, J.-K. Lee and R. A. Hatton, *Adv. Mater.*, 2023, **35**, 2300166.

[13] L.-Q. Yao, Y. Qin, X.-C. Li, Q. Xue, F. Liu, T. Cheng, G.-J. Li, X. Zhang and W.-Y. Lai, *InfoMat*, 2023, **5**, e12410.

[14] Z. Jiang, K. Fukuda, X. Xu, S. Park, D. Inoue, H. Jin, M. Saito, I. Osaka, K. Takimiya and T. Someya, *Adv. Mater.*, 2018, **30**, 1707526.

[15] M. Dressel and G. Grüner, Electrodynamics of Solids: Optical Properties of Electrons in Matter, Cambridge University Press, Cambridge, 2002.

[16] G. Haacke, J. Appl. Phys., 1976, 47, 4086-4089.

Table S7. Comparison of transmittance, sheet resistance, and figure of merits to previous studies with the transparent electrode of OLED device applications incorporating ultrathin metal films[1, 2], D/M/D multilayers[3, 4], conducting polymers[5, 6], AgNWs[7, 8], graphene[9, 10], evaporated[11, 12] or printed[13, 14] metal mesh.

Ref#	Electrode	Year	Fabrication method	Transmittance (%T)	Sheet resistance (ohm/sq)	Figure of merit (σ_{dc}/σ_{op}) [15]	Figure of merit (T^{10}/Rs, x10^{-3}) [16]
[1]	Ultrathin metal films	2020	TPBi/Ca/Ag 30/3/8-11nm Deposition	58.5-74.5	5.5-8.8	111.5-135.1	0.85-5.99
[2]		2025	ZnO/Yb:Ag(6%) 3/13-19nm Deposition	77.6-86.8	11.1-16.8	123.0-221.0	7.16-20.86
[3]	D/M/D multilayers	2016	MoOx/Au/MoOx 40/10-15/40nm E-beam evaporation	84.9-90.4	3.6-7.0	520.9-614.8	52.13-54.17
[4]		2008	IZTO/Ag/IZTO 30/12-20/30nm Sputtering	73.8-86.0	2.4-7.4	233.6-482.3	17.05-44.35
[5]	Conducting polymers	2017	PEDOT:PSS + ionic liquid (dry transfer)	91	67	63	5.81
[6]		2015	PEDOT:PSS + AgNW	80-90	8.5-123	28.3-187.9	2.83-12.63
[7]	Aligned AgNWs	2014	AgNW + reduced Ag ion ink	~95	27.5-39.5	183.7-263.9	15.16-21.77
[8]		2022	AgNW EHD printing	89.7-99.1	5.4-91	430.4-625.0	10.04-62.45
[9]	graphene	2015	Multilayer graphene (transfer)	84.9 (CsF:graphene)	118	18.7	1.65
[10]		2025	Graphene, CVD + transfer + PMMA removing in water	92.3-97.2	288-713.5	14.2-18.5	1.06-1.56
[11]	Evaporated metal mesh	2020	Au/Ag bilayer metal grid On crack template	85	5.2	428.2	37.86
[12]		2022	Cu deposition + lift off on crack template	76.5-93	3.4-13.4	380.7-386.8	20.19-36.12
[13]	Printed metal mesh	2023	AgNP Inkjet Printing	79.6-89.3	5.6-16.3	198.6-306.5	18.24-26.51
[14]		2017	Ag ink gravure off-set printing	81.8-86.5	4.0-19	131.9-446.0	12.34-33.53
Our work	Evaporated metal mesh	2025	Transfer printing + Selective deposition, Ag	93.6-99.0	1.11-4.44	5038.1-10756.4	204.6-463.5

References

[1] D. Yin, Z.-Y. Chen, N.-R. Jiang, Y.-F. Liu, Y.-G. Bi, X.-L. Zhang, W. Han, J. Feng and H.-B. Sun, *Org. Electron.*, 2020, **76**, 105494.

[2] E.-y. Choi, S.-C. Kang, K. Kim, S.-H. Lee, J.-B. Kim and J.-K. Song, *Light Sci. Appl.*, 2025, **14**, 62.

[3] M. Kim, C. Lim, D. Jeong, H.-S. Nam, J. Kim and J. Lee, *Org. Electron.*, 2016, **36**, 61-67.

[4] K.-H. Choi, H.-J. Nam, J.-A. Jeong, S.-W. Cho, H.-K. Kim, J.-W. Kang, D.-G. Kim and W.-J. Cho, *Appl. Phys. Lett.*, 2008, **92**, 223302.

[5] S. Kee, N. Kim, B. Park, B. S. Kim, S. Hong, J.-H. Lee, S. Jeong, A. Kim, S.-Y. Jang and K. Lee, *Adv. Mater.*, 2018, **30**, 1703437.

[6] M. Zhang, S. Höfle, J. Czolk, A. Mertens and A. Colsmann, *Nanoscale*, 2015, **7**, 20009-20014.

[7] R. E. Triambulo, H.-G. Cheong and J.-W. Park, *Org. Electron.*, 2014, **15**, 2685-2695.

[8] X. Feng, L. Wang, Y. Y. S. Huang, Y. Luo, J. Ba, H. H. Shi, Y. Pei, S. Zhang, Z. Zhang, X. Jia and B. Lu, *ACS Appl. Mater. Interfaces*, 2022, **14**, 39199-39210.

[9] J.-H. Chang, W.-H. Lin, P.-C. Wang, J.-I. Taur, T.-A. Ku, W.-T. Chen, S.-J. Yan and C.-I. Wu, *Sci. Rep.*, 2015, **5**, 9693.

[10] B. Kulyk, J. C. Germino, D. Gaspar, A. J. S. Fernandes, J. Deuermeier, A. F. Carvalho, A. F. da Cunha, L. M. N. Pereira, L. Pereira and F. M. Costa, *J. Mater. Chem. C*, 2025, **13**, 5855-5864.

[11] X. Huang, F. Zhang, Y. Liu and J. Leng, *ACS Appl. Mater. Interfaces*, 2020, **12**, 23236-23243.

[12] P. Liu, B. Huang, L. Peng, L. Liu, Q. Gao and Y. Wang, *Sci. Rep.*, 2022, **12**, 20494.

[13] L.-Q. Yao, Y. Qin, X.-C. Li, Q. Xue, F. Liu, T. Cheng, G.-J. Li, X. Zhang and W.-Y. Lai, *InfoMat*, 2023, **5**, e12410.

[14] S. Park, J. T. Lim, W.-Y. Jin, H. Lee, B.-H. Kwon, N. S. Cho, J.-H. Han, J.-W. Kang, S. Yoo and J.-I. Lee, *ACS Photonics*, 2017, **4**, 1114-1122.

[15] M. Dressel and G. Grüner, Electrodynamics of Solids: Optical Properties of Electrons in Matter, Cambridge University Press, Cambridge, 2002.

[16] G. Haacke, J. Appl. Phys., 1976, 47, 4086-4089.

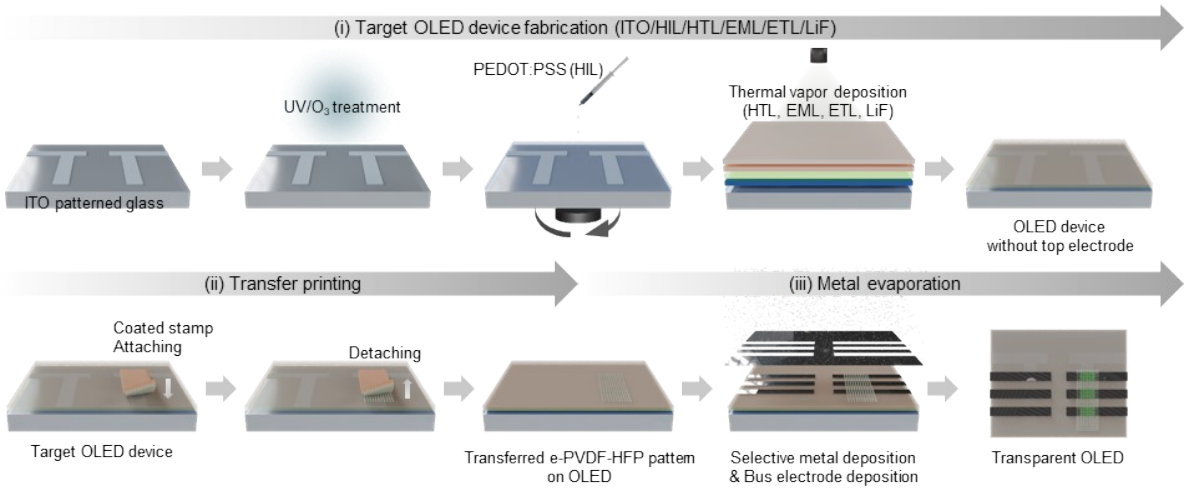

Figure S13. Fabrication process of transparent OLED with top metal mesh cathode

Table S8. Transmittance and sheet resistance of non-patterned Ag with different thicknesses

Ag deposition thickness (nm)	Transmittance (%T, at 550 nm)		Sheet resistance (ohm/sq)
	Raw data	Without substrate	
Glass substrate	91.7548	-	-
10	33.10	36.08	>2M (2019367.3)
12	36.61	39.90	16.784
15	34.09	37.15	5.171
20	33.10	36.07	2.006
25	24.85	27.08	1.383
30	16.67	18.17	1.000
50	3.660	3.989	0.535
100	0.05740	0.06256	0.213
200	-	-	0.1
300	-	-	0.064

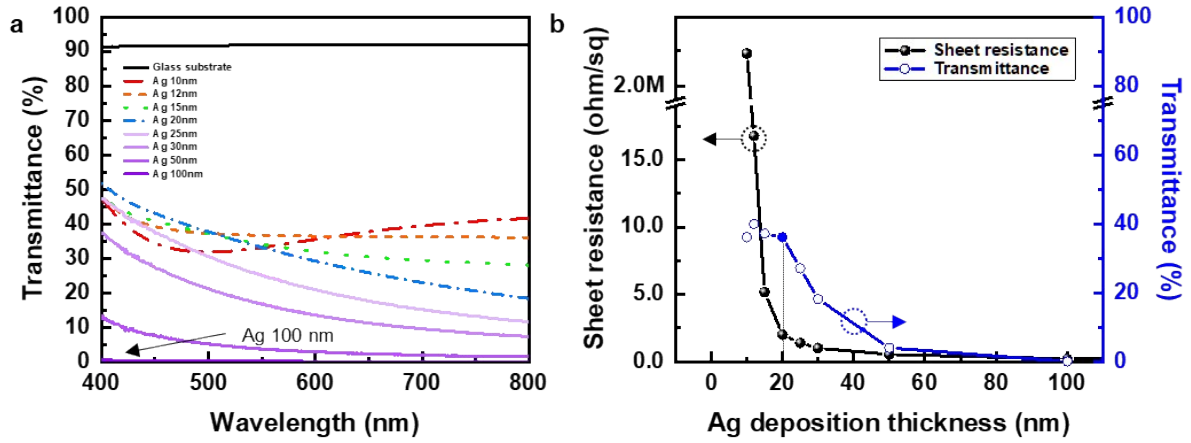

Figure S14. (a) Transmittance, (b) transmittance and sheet resistance of non-patterned Ag with different thicknesses

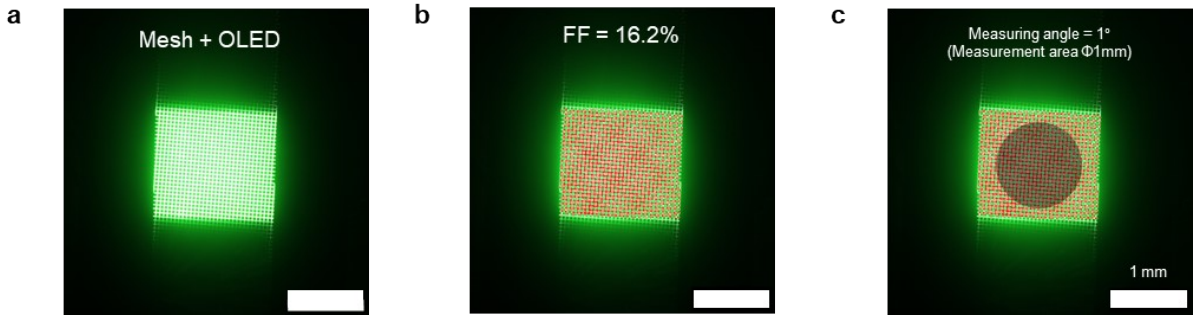

Figure S15. Luminance measurement area and areal fill factor extracted from emission image (Scale bar = 1 mm) (a) Emission image taken with average current density of 22.3 mA cm^{-1} (0.5 mA) (b) Emission area analysis using ImageJ plugin, highlighted in red (c) luminance measurement area (annotated circle), measuring angle = 1°

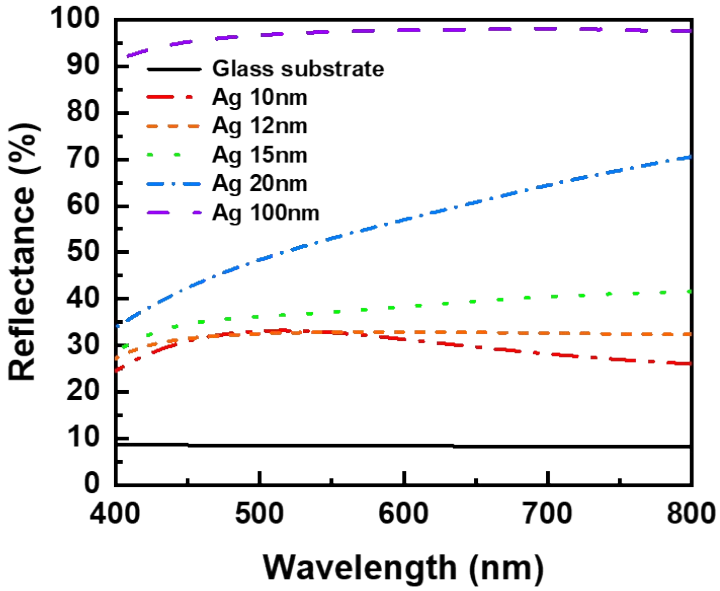

Figure S16. Reflectance of non-patterned Ag with different thickness

Table S9. Reflectance of non-patterned Ag with different thickness

Ag deposition thickness (nm)	Reflectance (%R, at 550 nm)
Glass substrate	8.43
10	32.77
12	32.85
15	37.16
20	52.99
100	97.39

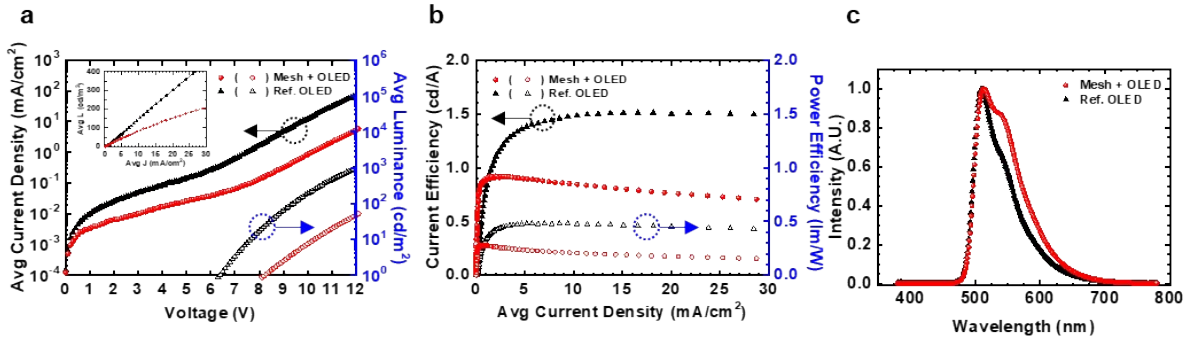

Figure S17. OLED device characteristics measured from top side (a) J-V-L graph (inset : J-L graph) (b) Current and power efficiencies (c) EL spectra

Table S10. OLED device characteristics measured from top and bottom side

	Max. CE (cd/A) / PE (lm/W) / EQE (%)		Average L (cd/m^2) At J_{avg} = 25 mA/cm^2			λ_{max} (nm)		CIE (x,y)	
	Top	Bottom	Top	Bottom	Top + Bottom	Top	Bottom	Top	Bottom
Mesh + OLED	0.92 / 0.28 / 0.26	14.2 / 4.3 / 4.2	185 (14v)	2884	3069	513	511	(0.32, 0.62)	(0.30, 0.62)
Ref. OLED	1.5 / 0.48 / 0.44	8.7 / 2.7 / 2.5	391 (10.8v)	2238	2629	510	511	(0.29,0.62)	(0.30, 0.62)

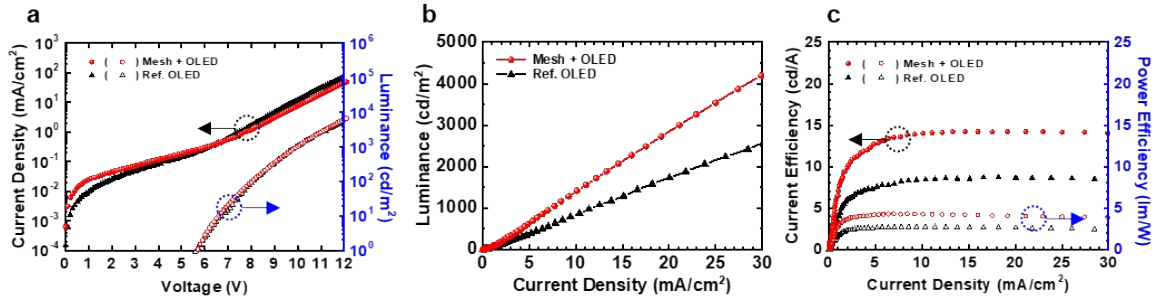

Figure S18. Areal fill factor compensation of average current density and average luminance (a) J-V-L graph with areal fill factor compensation (b) J-L graph with areal fill factor compensation (c) Current and power efficiencies with areal fill factor compensation

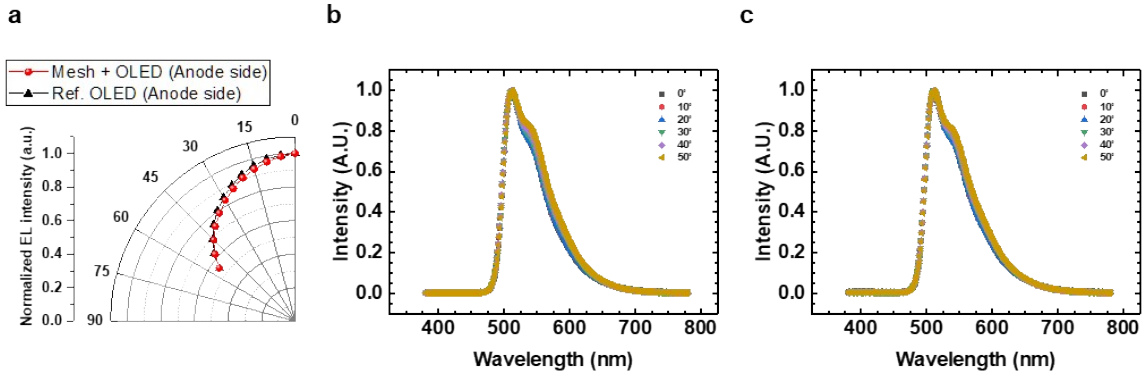

Figure S19. (a) Angular-dependent electroluminescence (EL) properties of the devices with mesh-patterned and planar thin silver top electrodes. (b)-(c) Angular-dependent EL spectra of the device (b) with mesh-patterned silver top electrodes and (c) with planar thin silver top electrodes (Ref. OLED). All results ((a)-(c)) were measured from the bottom ITO (anode) side.

Table S11. Comparison of OLED device characteristics to previous studies with transparent electrodes incorporating ultrathin metal film[1, 2], D/M/D multilayer[3, 4], conducting polymer[5, 6], AgNW[7, 8], graphene[9, 10], evaporated[11, 12] or printed[13, 14] metal mesh.

Ref#	Electrode	Year	OLED device demonstration				Device performance		
			Transparency	Emission Layer	Bottom Electrode	Top Electrode	Max. L (cd/m²)	Max. CE (cd/A)	Max. EQE (%)
[1]	Ultrathin metal film	2020	O	mCP:Ir(ppy)3, green	Thin metal film MoO3/Au	Thin metal film TPBi/Ca/Ag/NPB	17900 (bottom) 15300 (top)	12.4 (bottom) 12.8 (top)	-
[2]		2025	O	TCTA:Bphen:Ir(ppy)3, green	ITO	Thin metal film ZnO/Yb:Ag(6%)/NPB	50227 (bottom) 19486 (top)	22.1 (bottom) 10.5 (top)	-
[3]	D/M/D multilayers	2016	X	Alq3:C545T, green	MoOx/Au/MoOx	Al 150nm	-	11.46	-
[4]		2008	X	CBP:Ir(ppy)3, green	IZTO/Ag/IZTO	Al 100nm	-	-	-
[5]	Conducting polymer	2017	O	PDY-132, yellow	PEDOT:PSS	PEDOT:PSS (transfer)	3200	2.8 (total)	-
			O	SPW-111, white			1200	2.7 (total)	-
[6]		2015	O	Super Yellow, yellow	PEDOT:PSS	PEDOT:PSS/AgNW	at 20mA/cm2: 2260 (bottom) 1760 (top)	11.3 (bottom) 8.3 (top)	-
			O	Merck Blue, blue			at 20mA/cm2: 270 (bottom) 230 (top)	1.4 (bottom) 1.1 (top)	-
[7]	Aligned AgNW	2014	X	Red polymer (livilux), red	Random AgNW Roll-to-roll coating	Al 100nm	400	-	-
[8]		2022	X	Alq3, green	Aligned AgNW microgrid EHD printing	Al 100nm	-	27.2 (at 92cd/m²)	-
[9]	graphene	2015	O	PVK:Firpic, blue	ITO	CsF:graphene (transfer)	1034	3.1	-
[10]		2025	X	PVK:mCP:TXO-TPA, green TADF	Graphene	Al 100 nm	920	-	1.20
[11]	Evaporated metal mesh	2020	X	MEH-PPV:PFO, white	Evaporated metal mesh Au/Ag, crack-based	Al 150nm	-	4.3	-
[12]		2022	X	Alq3, green	Evaporated metal mesh Cu, crack-based	Al 100nm	1587	0.8	-
[13]	Printed metal mesh	2023	O	PO-01, red Flrpic, sky blue (white)	**Embedded mesh** AgNP, inkjet printing	Thin metal film Al/Ag	8343 (bottom)	16.5 (bottom)	-
[14]		2017	O	(Ir(ppy)2(m-bppy)):PGH02, yellow	ITO	**Embedded mesh (lamination)** Ag ink paste, PEDOT:PSS gravure off-set printing	2880 (bottom) 3263 (top)	24.5 (bottom) 25.8 (top)	7.9 (bottom) 7.4 (top)
Our work	Evaporated metal mesh	2025	O	CBP:Ir(ppy)3, green	ITO	Evaporated Metal mesh	1963-4224 (bottom) 92-267 (top)	9.7-14.2 (bottom) 0.59-0.92 (top)	2.9-4.2 (bottom) 0.17-0.26 (top)

References

[1] D. Yin, Z.-Y. Chen, N.-R. Jiang, Y.-F. Liu, Y.-G. Bi, X.-L. Zhang, W. Han, J. Feng and H.-B. Sun, *Org. Electron.*, 2020, **76**, 105494.

[2] E.-y. Choi, S.-C. Kang, K. Kim, S.-H. Lee, J.-B. Kim and J.-K. Song, *Light Sci. Appl.*, 2025, **14**, 62.

[3] M. Kim, C. Lim, D. Jeong, H.-S. Nam, J. Kim and J. Lee, *Org. Electron.*, 2016, **36**, 61-67.

[4] K.-H. Choi, H.-J. Nam, J.-A. Jeong, S.-W. Cho, H.-K. Kim, J.-W. Kang, D.-G. Kim and W.-J. Cho, *Appl. Phys. Lett.*, 2008, **92**, 223302.

[5] S. Kee, N. Kim, B. Park, B. S. Kim, S. Hong, J.-H. Lee, S. Jeong, A. Kim, S.-Y. Jang and K. Lee, *Adv. Mater.*, 2018, **30**, 1703437.

[6] M. Zhang, S. Höfle, J. Czolk, A. Mertens and A. Colsmann, *Nanoscale*, 2015, **7**, 20009-20014.

[7] R. E. Triambulo, H.-G. Cheong and J.-W. Park, *Org. Electron.*, 2014, **15**, 2685-2695.

[8] X. Feng, L. Wang, Y. Y. S. Huang, Y. Luo, J. Ba, H. H. Shi, Y. Pei, S. Zhang, Z. Zhang, X. Jia and B. Lu, *ACS Appl. Mater. Interfaces*, 2022, **14**, 39199-39210.

[9] J.-H. Chang, W.-H. Lin, P.-C. Wang, J.-I. Taur, T.-A. Ku, W.-T. Chen, S.-J. Yan and C.-I. Wu, *Sci. Rep.*, 2015, **5**, 9693.

[10] B. Kulyk, J. C. Germino, D. Gaspar, A. J. S. Fernandes, J. Deuermeier, A. F. Carvalho, A. F. da Cunha, L. M. N. Pereira, L. Pereira and F. M. Costa, *J. Mater. Chem. C*, 2025, **13**, 5855-5864.

[11] X. Huang, F. Zhang, Y. Liu and J. Leng, *ACS Appl. Mater. Interfaces*, 2020, **12**, 23236-23243.

[12] P. Liu, B. Huang, L. Peng, L. Liu, Q. Gao and Y. Wang, *Sci. Rep.*, 2022, **12**, 20494.

[13] L.-Q. Yao, Y. Qin, X.-C. Li, Q. Xue, F. Liu, T. Cheng, G.-J. Li, X. Zhang and W.-Y. Lai, *InfoMat*, 2023, **5**, e12410.

[14] S. Park, J. T. Lim, W.-Y. Jin, H. Lee, B.-H. Kwon, N. S. Cho, J.-H. Han, J.-W. Kang, S. Yoo and J.-I. Lee, *ACS Photonics*, 2017, **4**, 1114-1122.

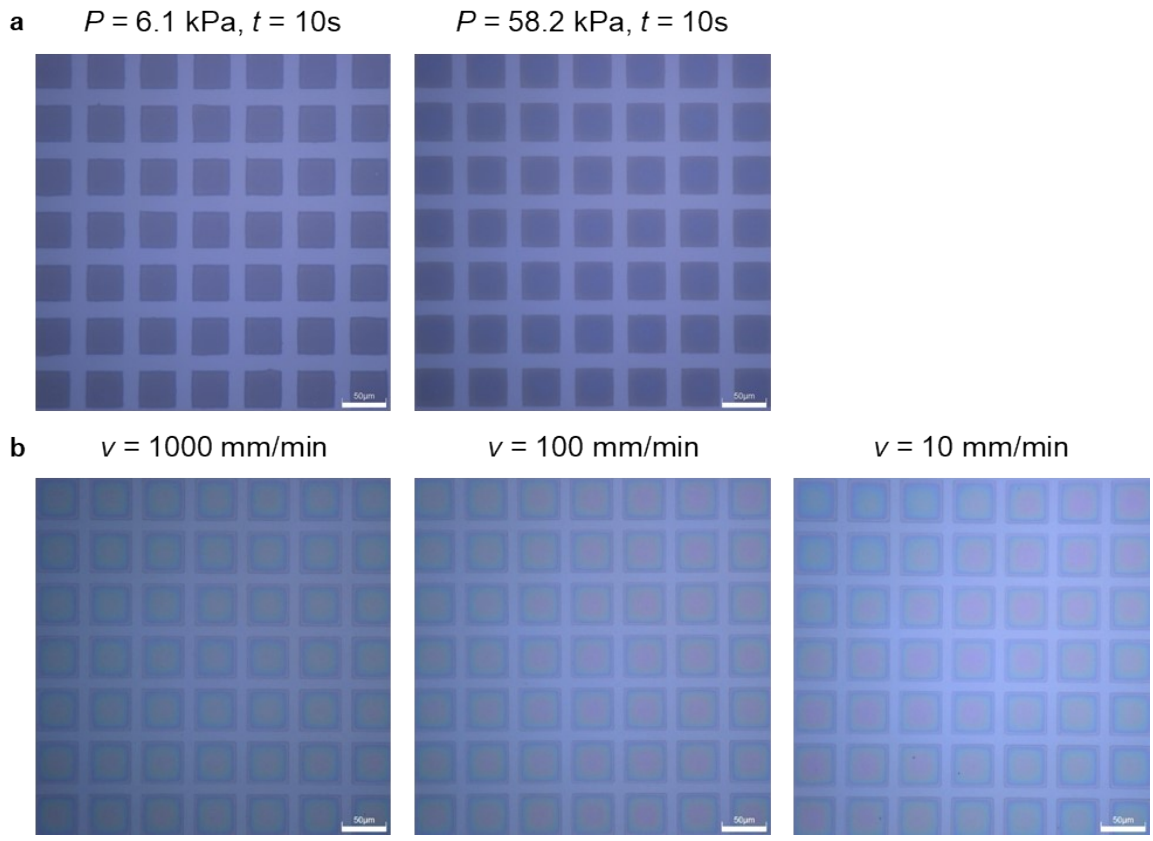

Figure S20. Optical images of transferred e-PVDF-HFP patterns on glass, (a) with different pressure (P) applied during the pressing period (t) of the transfer printing process, or (b) different releasing speeds (v), using an automatic stage. (Ink concentration: 5 wt% for (a), 10 wt% for (b))